Conceptual design of a scintillator based fast-ion loss detector for the Wendelstein 7-X stellarator

A. Jansen van Vuuren[1], S. A. Lazerson[2], A. LeViness[3], M. Garcia-Munoz[1,4], D. Gates[3], J. Galdon-Quiroga[1], J. Hidalgo-Salaverri[4,5], J. Rueda-Rueda[1,4], J. Garcia-Dominguez[4,5] J. Ayllon-Guerola[4,5] and the Wendelstein 7-X Team[†]

[1] *Dept. of Atomic, Molecular and Nuclear Physics, University of Seville, Spain*
[2] *Max-Planck Institute for Plasma Physics, 17489 Greifswald, Germany*
[3] *Princeton Plasma Physics Laboratory, Princeton, NJ*
[4] *Centro Nacional de Aceleradores (U. Sevilla, CSIC, J. de Andalucia), Seville, Spain*
[5] *Dept. of Mechanical Engineering and Manufacturing, University of Seville, Spain*

***Abstract*—A conceptual design of a scintillator based fast-ion loss detector has been developed for the Wendelstein 7-X stellarator. Simulations using the Monte Carlo codes ASCOT5 and BEAMS3D have been performed to calculate the expected flux of neutral beam injection (NBI) generated fast hydrogen ions onto the conceptual detector probe head. These fast-ion loss fluxes have been calculated for several magnetic field configurations as well as probe insertion positions. At the maximum insertion position both co and counter-going losses with high incident pitch angles are observed, however at retracted positions only co-going fast ions reach the probe head. The FILDSIM code has been used to optimise the geometry of the detector entrance and collimating elements to achieve a wide velocity space coverage as well as a high velocity-space resolution. A synthetic FILD signal is calculated for the expected loss distribution via forward modelling using the instrument response function. The synthetic signal is found to largely retain the velocity space features of the loss distribution.**

***Index Terms*—Magnetic confinement fusion, Fast-ion loss detector, fast ions, Wendelstein 7-X**

I. Introduction

The demonstration of good fast-ion confinement in stellarators is important in order for these devices to be viable options for future fusion reactors. This is one of the main goals of the Wendelstein 7-X stellarator (W7-X), which is optimised for good fast-ion confinement [1], [2], particularly at high plasma pressure [3]. Importantly, fast-ion diagnostics capable of inferring the fast-ion confinement properties of W7-X are required. Fast-ion loss detectors (FILD) are especially well suited for this task and have been employed in multiple magnetic confinement devices.

Two different types of FILDs exist, namely Faraday cup (FC) and scintillator based detectors. FC-FILDs rely on measuring the current induced by fast ions impinging on a conductive plate, with such a detector presently installed in W7-X [4]. Scintillator based FILDs on the other hand measure the light emitted by fast ions impinging on a plate covered with scintillating material [5]. Scintillator based FILDs provide significantly higher velocity-space resolution and signal-to-noise ratios (SNR) as compared to FC-FILDs. Furthermore, these detectors are immune from electromagnetic pickup which FC-FILDs can be susceptible to [6]. Importantly, by using fast response scintillating materials [7] and high speed photon acquisition systems, these type of detectors can measure down to the Alfvén Eigenmode timescales ($\sim$ 1 MHz) making them excellent tools to investigate the various mechanisms responsible for fast-ion transport [8].

A scintillator based FILD system is currently being developed to be installed on W7-X during the OP2 campaign. The system is being developed by the Princeton Plasma Physics Laboratory in collaboration with the Max-Planck Institute of Plasma Physics and the University of Seville. Here, a conceptual design and evaluation of the detector in its allocated port position is presented. The paper is structured as follows, first a description of the conceptual detector is presented in section II followed by modelling of the expected fast-ion losses onto the model FILD probe head in section III. Next, the design and optimisation of the probe head, guided by the aforementioned modelling results, is described in section IV. Finally, in section V the expected signal is calculated for the detector by means of forward modelling.

II. A conceptual scintillator based FILD system for W7-X

Figure 1 shows the conceptual design of the planned FILD system. The probe head, drawn in cyan, is positioned atop a reciprocating manipulator arm (orange) in the assigned port. The system will attach to the lowermost of three sub flanges in the AEN21 port, with the centre flange supporting a separate Faraday cup based FILD detector [9]. The manipulator arm will contain an optical system to relay light produced by fast ions impacting on scintillator plate to ex-vessel imaging systems, such as a charge coupled device camera and an array of photomultiplier tubes. Furthermore, the manipulator arm will guide water cooling tubes to allow for active cooling of the probe head, which must be able to withstand up to $200\,\mathrm{kW\,m^{-2}}$ of stray electron cyclotron resonance heating (ECRH) for up to 100 s. Motion of the reciprocating system will be achieved through the use of a pneumatic drive system.

The conceptual detector probe head is shown in figure 1b and illustrates the working principle of the detector, which

[†] See author list of T. Sunn Pedersen *et al.* Nucl. Fusion **62** 042022

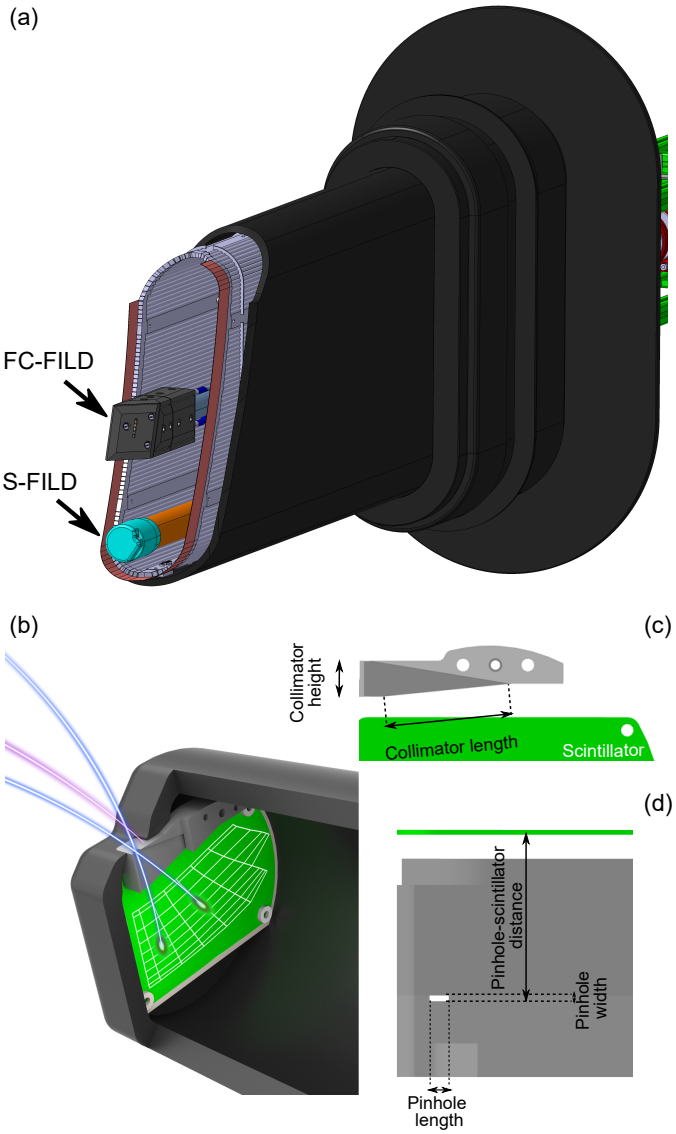

Fig. 1. a) Illustration of the conceptual scintillator based FILD system (S-FILD) for W7-X in the planned port position. The new S-FILD will share the port with a Faraday cup based FILD (FC-FILD). b) Cut away illustration of the FILD probe head showing the scintillator plate (in green). Illustration of the detector collimator (c) as observed from the camera view and (d) a top down view of probe head pinhole entrance.

functions as a phase-space spectrometer. Escaping fast ions reaching the detector aperture, a rectangular slit like opening, pass through collimating elements to reach a scintillator plate. The strike location on the scintillator plate is determined both by the gyro-radius, which is related to the particle perpendicular energy (E), and pitch angle of the ion. The impact of the ion on the scintillator plate produces light at the strike location that is measured.

III. Modelling of the expected fast-ion losses

Modelling using the full fast-ion orbit code ASCOT5 [10], [11] has been performed to determine the expected fast-ion losses onto the planned FILD probe head. The ASCOT5 simulations were provided with the bulk plasma profiles, equilibrium magnetic field, 3D wall geometry and fast-ion birth distributions as input. The input profiles included the electron density (n_e) and temperature (T_e), the ion temperature (T_i) as well as the effective charge (Z_{eff}) and electric field.

The input kinetic profiles provided take the form $n_e(s) = n_{e0} \cdot (3 - s^3)/3$ and $T_{e,i}(s) = T_{e,i0} \cdot (1 - s^{0.5})$, with $s = \rho^2$, where ρ refers to the normalised plasma radius. The profile shapes are approximations of the experimentally measured plasma profiles for a large set of ECRH heated discharges with NBI from the OP2.1b campaign [12]. In this work plasma cases with moderate core plasma density of $n_{e0} = 5 \cdot 10^{-19}\mathrm{m}^{-3}$ and temperatures of $T_{e0} = 3\,\mathrm{keV}$ and $T_{i0} = 1.6\,\mathrm{keV}$, were modelled. The plasma species mix was considered to only consist of hydrogen thus the Z_{eff} profile was set to 1, and the impact of impurities has not been considered in this work.

The input equilibria were calculated using VMEC [13] with the boundary set by fits to the vacuum last closed flux surface (LCFS). The fields in the region outside the LCFS were constructed using a linear superposition of vacuum fields and the plasma response calculated from the virtual casing principle described in [14]. In this work the standard (EIM), high iota (FTM) and high mirror (KJM) magnetic field configurations at W7-X were examined. Given the input kinetic profiles and equilibria the electric field profiles were calculated using the neoclassical transport code NEOTRANSP. Lastly, given the input kinetic profiles and equilibrium the NBI birth distributions were calculated for all 8 NBI sources [15] using the BEAMS3D code [16]. Here, BEAMS3D is used as it has been carefully benchmarked against experiments at W7-X [17], [18].

To assess the expected losses onto the planned FILD, a model probe head has been included in the ASCOT5 3D wall, as shown in figure 2a. Several probe head insertion positions of the probe head were investigated, from the parking position which is around $30\,\mathrm{cm}$ from the LCFS up to the maximum insertion position about $5\,\mathrm{cm}$ from the LCFS.

The modelling methodology used in this work follows a similar approach to that described in [19]. First, gyro-centre slowing-down simulations are performed using ASCOT5. In this first step the BEAMS3D calculated markers (numbering $\sim 10^6$) are followed using ASCOT5 for $20\,\mathrm{ms}$ or until the markers reach the LCFS. The vast majority ($> 99\,\%$) of markers that do not reach the LCFS within $20\,\mathrm{ms}$ are found to thermalise as confirmed by full slowing down simulations. Here, a marker is considered to have thermalised when its energy is less than $\frac{3}{2}$ the local ion temperature. As the thermalisation time can be as long as $100\,\mathrm{ms}$ a significant amount of computational time is saved by disregarding these markers which will never reach a FILD detector. In the next step the markers that have reached the LCFS are relaunched in a separate simulation, however now their full orbit trajectories are followed. These markers (numbering $\sim 10^5$) are initiated from their respective positions on the LCFS and with their last recorded velocity. The markers are followed until they collide with wall elements (see figure 2a) or are thermalised.

Markers are observed to reach the FILD probe head in all magnetic field configurations. The flux of markers incident

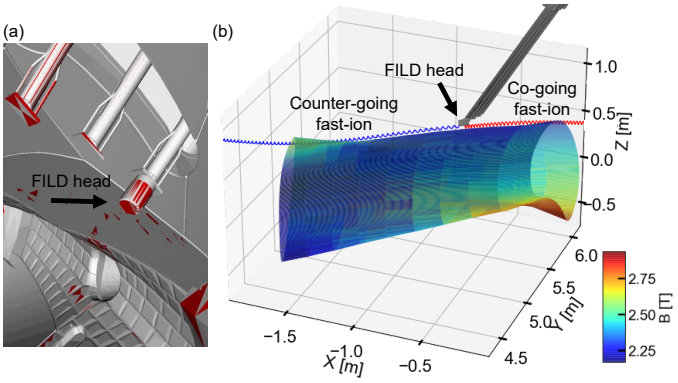

Fig. 2. (a) Illustration of the model FILD probe head in the ASCOT5 input wall geometry. The coloured mesh elements indicate collisions with fast-ion markers. (b) Illustration of the input LCFS geometry in the region in front of the FILD system with example fast-ion orbits calculated by ASCOT5 that collide with the detector.

onto the probe head is found to be dependent on the magnetic field configuration and the position of the probe head with respect to the LCFS. The EIM configuration is observed to yield the largest flux of markers, followed by the KJM and FTM configurations. The velocity space distribution of markers reaching the probe head is found to be similar for all configurations. Both co- and counter-going markers are observed to reach the probe head at its maximum insertion position, with example orbits shown in figure 2b. Here, co- and counter going refers to the travel direction of the markers with respect to the magnetic field. Co-going markers travel along the magnetic field direction while counter-going markers travel in the opposing direction. As can be seen in figure 3a, the velocity-space distribution of these markers consist of two narrow pitch populations around $\sim 75°$ and $\sim 120°$, corresponding to the co- and counter-going markers respectively. Simulations with the probe head at increasingly retracted positions find that the flux of counter-going markers quickly decay such that counter-going markers do not reach the probe for probe head positions further than around $8\,\mathrm{cm}$ from the LCFS, as can be seen in figure 3b.

As can be seen in figures 3a and b markers with energies around the full ($55\,\mathrm{keV}$), half and third beam-energy components are clearly observable. Additionally, markers with energies below the injection energies are observed as tails in the distribution indicating not all losses correspond to prompt losses. The gyro-radii of the markers at the probe head, where the magnetic field is around $2.3\,\mathrm{T}$, range between 0.5 and $1.6\,\mathrm{cm}$.

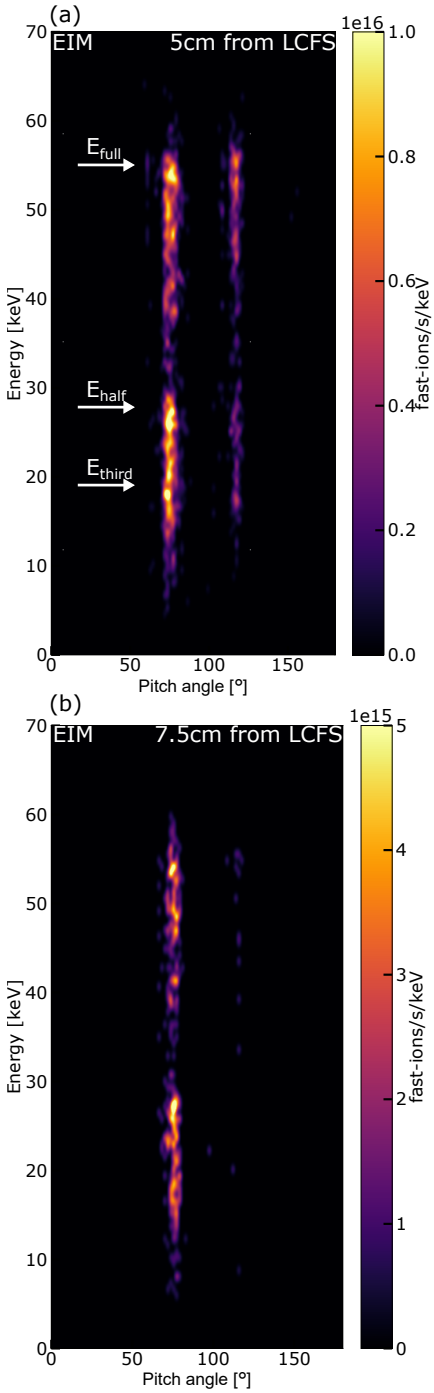

Fig. 3. Velocity-space distribution of fast-ion markers reaching the FILD probe head at (a) $5\,\mathrm{cm}$ and (b) $7.5\,\mathrm{cm}$ from the LCFS, respectively, in the EIM configuration.

IV. Design optimisation of the FILD probe head

A probe head with collimating elements optimised to measure the ASCOT5 calculated loss distribution has been investigated using the FILDSIM code [20]. FILDSIM is a Monte Carlo code that tracks the helical trajectory of fast ions within a FILD detector as they pass through collimating elements and impinge onto a scintillator plate. The code allows to construct strike maps relating the gyro-radii and pitch angle of particles to real space coordinates on the scintillator plate. Furthermore, FILDSIM allows to calculate the pitch and gyro-radius resolution of a detector as well as the collimating factor. Here, the collimating factor is defined as the fraction of particles that are able reach the scintillator plate over the number of particles that enter the detector. Note, the collimating factor is a function of the particle gyro-radius and pitch angle. This information allows to construct an instrument response function for a given detector design

that can be used to calculate synthetic signals from theoretical loss distributions.

The instrument response function is determined by the probe head design, including properties such as the opening slit dimensions and collimator geometry as well as the detector alignment with respect to the local magnetic field vector. During this work parametric scans of the detector slit size, collimating geometry and pinhole to scintillator distance have been performed. These design parameters are illustrated in figure 1c and d. The optimal design parameters were determined by three criteria with decreasing order of importance. First, the design parameters should allow the detector to measure escaping fast ions with pitch angles ranging between 25 and 85° and gyro-radii above 0.5 cm. Secondly, the maximum velocity space resolution in terms of pitch and gyro-radius is desired which is compatible with the first criteria. Thirdly, the maximum collimating factor that is compatible with the first two criteria is desired.

Scans of the probe design parameters were carried out. Here, the detector was aligned such that the scintillator plate and collimating elements were perfectly parallel with the local magnetic field. As an example of the impact that a given parameter has on the detector's response, figure 4 demonstrates the relation between slit width and the detector resolution. As can be seen for decreasing slit width the gyro-radius resolution decreases, a desirable feature for the detector. However, below 0.08 cm the minimum gyro-radius of particles able to reach the scintillator plate increases above 0.5 cm. This is undesirable as the minimum gyro-radius the detector should be able to measure is 0.5 cm. Looking at figure 4c the slit width has a negligible impact on the pitch resolution which is on the order of 1°. Decreasing the slit width does decrease the detector collimating factor, however, this is of secondary importance with respect to the better gyro resolution gained from a smaller slit width. Thus the value of slit width that has the lowest resolution while still allowing to measure particles with gyro radii >0.5 cm is considered to be the optimal choice. At this value the collimating factor is expected to still be satisfactory at 6 %.

TABLE I
OPTIMAL FILD HEAD DESIGN PARAMETERS.

Design Parameter	Value [cm]
Pinhole Length	0.1
Pinhole Width	0.08
Pinhole Scintillator Distance	0.8
Collimator Height	0.4
Collimator Width	2.0
Scintillator Size	4.0×4.0

Table I shows the optimal values obtained for the other design parameters. Figure 5a shows the corresponding strike map. As can be seen the detector solution offers a large pitch and gyro-radius range, suitable to measure the expected neoclassical NBI fast-ion losses. The corresponding particle energies range between 15 and 400 keV for H and 8 and 200 keV for D ions. The large energy range means that ions accelerated by ion cyclotron resonance heating (ICRH) [21] may also be measured by the planned FILD.

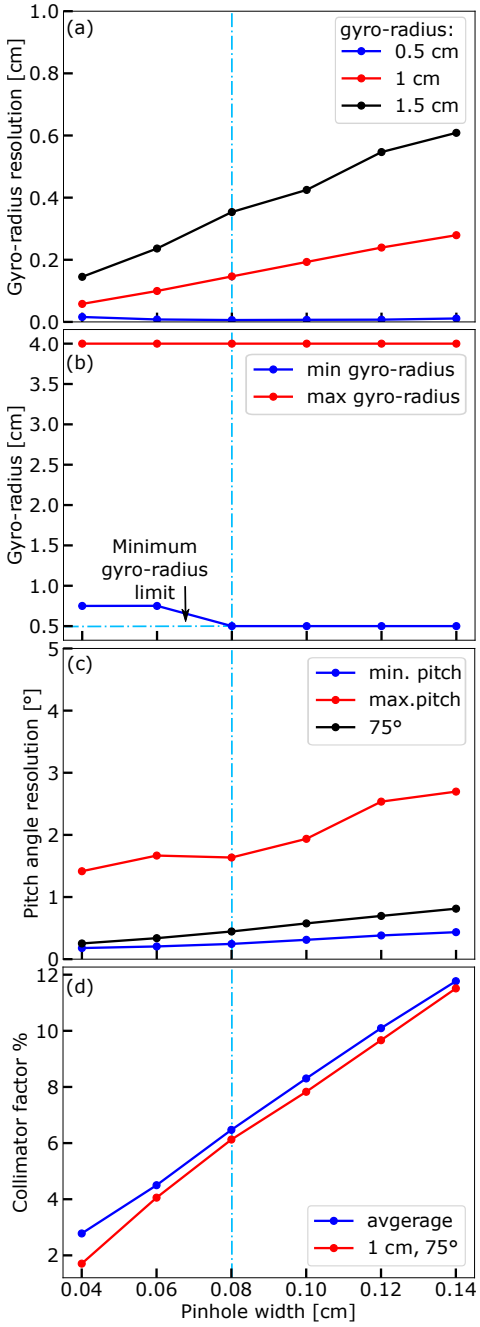

Fig. 4. Scan of the detector pinhole width showing the impact on the gyro-radius (a) resolution and (b) range as well as the pitch (c) resolution and the (d) detector collimating factor. The vertical dashed-dotted cyan lines indicate the optimal value of the pinhole width. The horizontal cyan line in (b) indicates the minimum gyro-radius constraint imposed.

Figure 5b shows the detector collimating factor which is found to be above 5 % across a large part of the scintillator, including the region where the NBI losses are expected. As seen in fig 5c, a high gyro-radius resolution is obtained particularly at low gyro radii (< 1 cm). The strike positions of these fast ions have a very narrow spatial spread on the scintillator plate. For increasing gyro radii values an increasing overlap in strike positions is observed along the gyro-radius direction. However, for fast ions with gyro radii below ∼2 cm the strike-point distribution peaks are still well separated.

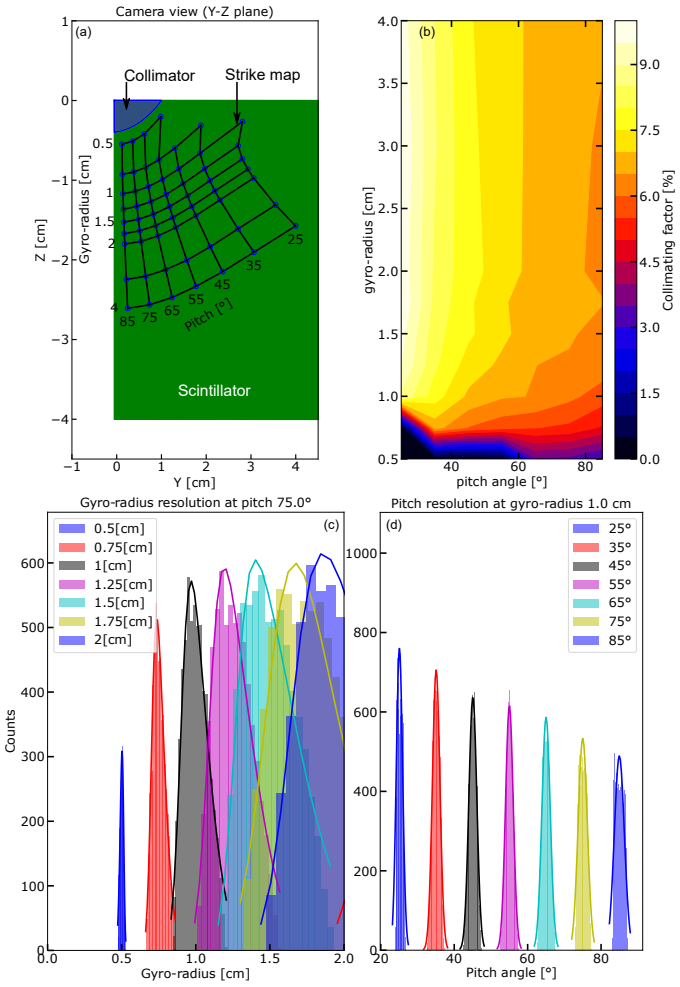

Fig. 5. FILDSIM calculated (a) strike map, (b) collimating factor, (c) gyro-radius and (d) pitch angle resolution for a FILD detector with design parameters given in table I.

Furthermore, as seen in fig 5d, a high pitch resolution across the full pitch angle range is achieved for the detector.

Lastly, FILDSIM has been used to investigate the design parameters of a probe head capable of measuring both co- and counter-going fast ions. Here, a double slit configuration is assessed, with the two slits positioned at opposite sides of the probe head, as shown in figure 6a. Figure 6b shows the corresponding strike maps resulting from particles passing through the two collimators. The FILDSIM calculations show, for the same slit and collimator dimensions as in table I, a scintillator plate with a width of at least $8\,\mathrm{cm}$ is needed to avoid excessive overlapping of the strike maps.

V. Modelling of the expected FILD signal

Using the instrument function calculated from FILDSIM a synthetic signal is calculated for the detector given the theoretical loss distribution. Figure 7 shows the synthetic signal corresponding to the loss distribution of markers in the EIM configuration calculated for the detector $7.5\,\mathrm{cm}$ from the LCFS. As can be seen the pitch distribution of the losses are well conserved, while a slight smearing out of the markers in the gyro-radius direction is observed. The gyro-radius

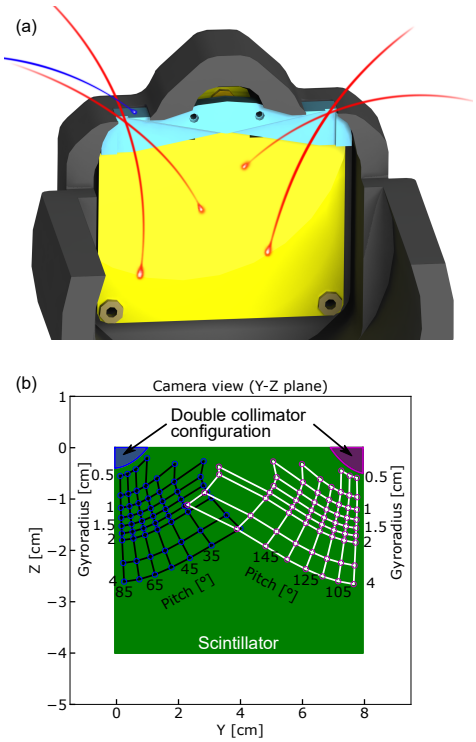

Fig. 6. a) Illustration of a double slit configuration FILD head to allow for measuring both co- and counter going fast-ion losses. b) The corresponding FILDSIM calculated strike maps for a double slit FILD head.

smearing is expected and does not excessively distort features in the loss distribution. As can be seen the full beam energy prompt losses are clearly distinguishable from the second and third beam energy losses. The latter components however are not clearly distinguishable.

VI. Conclusion

Modelling of the expected fast-ion loss fluxes onto a model FILD probe head have been carried out using the BEAMS3D and ASCOT5 codes. These are assessed for three magnetic field configurations of W7-X, namely the STD, KJM and FTM. The loss flux is found to be largest in the STD magnetic configuration followed by the KJM and FTM configurations. The loss flux onto the probe consists mainly of high pitch angle fast ions, with both co going and counter going losses observed when the probe head is at its closest position to the LCFS, $5\,\mathrm{cm}$. However, the flux of counter going losses rapidly decays with increasing distance of the probe head from the LCFS. At distances further than $7.5\,\mathrm{cm}$ mainly co going losses are observed. Guided by the expected velocity-space distribution of the losses, the optimal design parameters for a detector have been determined using the FILDSIM code. Here, maximal velocity-space coverage, high detector resolution and large collimating factors were the criteria optimised for by varying a set of design parameters, including the detector slit and collimator geometry. Finally, the FILDSIM code was used to determine the expected instrument response of the resulting detector which was used to calculate synthetic signals via forward modelling. The synthetic signals are observed to retain the pitch angle distribution of the expected losses, with a minor

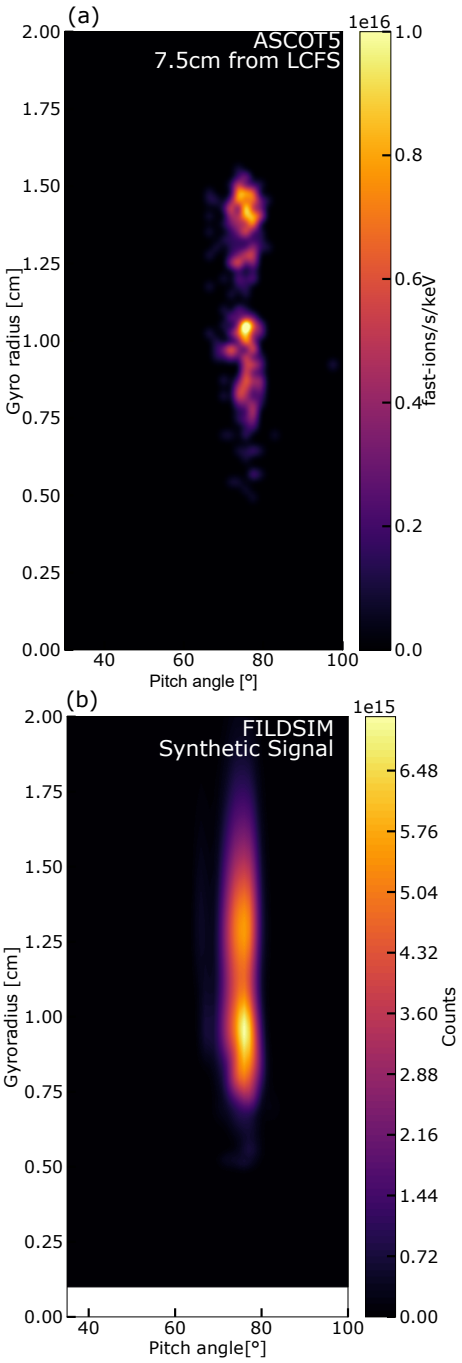

Fig. 7. Comparison of the (a) ASCOT5 calculated fast-ion loss distribution (for the EIM configuration) to the corresponding (b) synthetic signal calculated using FILDSIM for the optimised detector.

smearing out of losses in the gyro-radius direction. However, this is sufficiently low as features such as peaks of losses at the beam injection energies can be distinguished.

Acknowledgements

This work has been carried out within the framework of the EUROfusion Consortium, funded by the European Union via the Euratom Research and Training Programme(Grant Agreement No 101052200 — EUROfusion). Views and opinions expressed are however those of the author(s) only and do not necessarily reflect those of the European Union or the European Commission. Neither the European Union nor the European Commission can be held responsible for them. J.Galdon-Quiroga acknowledges the support from the Spanish Ministry of Science and Innovation under grant no. FJC-2019-041092-I

References

[1] W. Lotz, P. Merkel, J. Nuhrenberg, and E. Strumberger, "Collisionless alpha -particle confinement in stellarators," *Plasma Physics and Controlled Fusion*, vol. 34, no. 6, pp. 1037–1052, jun 1992.

[2] M. Drevlak, J. Geiger, P. Helander, and Y. Turkin, "Fast particle confinement with optimized coil currents in the w7-x stellarator," *Nuclear Fusion*, vol. 54, no. 7, p. 073002, apr 2014.

[3] E. Strumberger, "Deposition patterns of fast ions on plasma facing components in w7-x," *Nuclear Fusion*, vol. 40, no. 10, pp. 1697–1713, oct 2000.

[4] K. Ogawa, S. Bozhenkov, S. Äkäslompolo, C. Killer, O. Grulke, D. Nicolai, G. Satheeswaran, M. Isobe, M. Osakabe, M. Yokoyama, and R. Wolf, "Energy-and-pitch-angle-resolved escaping beam ion measurements by faraday-cup-based fast-ion loss detector in wendelstein 7-x," *Journal of Instrumentation*, vol. 14, no. 09, pp. C09 021–C09 021, sep 2019.

[5] S. Zweben, "Pitch angle resolved measurements of escaping charged fusion products in TFTR," *Nuclear Fusion*, vol. 29, no. 5, pp. 825–833, may 1989.

[6] P. J. Bonofiglo, V. Kiptily, A. Horton, P. Beaumont, R. Ellis, F. E. Cecil, and M. Podesta, "Improvements to the faraday cup fast ion loss detector and magnetohydrodynamic induced fast ion loss measurements in joint european torus plasmas," *Review of Scientific Instruments*, vol. 91, no. 9, p. 093502, 2020. [Online]. Available: https://doi.org/10.1063/5.0014278

[7] M. Jiménez-Ramos *et al.*, "Characterization of scintillator materials for fast-ion loss detectors in nuclear fusion reactors," *Nuclear Instruments and Methods in Physics Research Section B: Beam Interactions with Materials and Atoms*, vol. 332, pp. 216–219, 2014, 21st International Conference on Ion Beam Analysis.

[8] M. García-Muñoz, H.-U. Fahrbach, and H. Zohm, "Scintillator based detector for fast-ion losses induced by magnetohydrodynamic instabilities in the asdex upgrade tokamak," *Review of Scientific Instruments*, vol. 80, no. 5, p. 053503, 2009.

[9] S. A. Lazerson *et al.*, "Development of a faraday cup fast ion loss detector for kev beam ions," *Review of Scientific Instruments*, vol. 90, no. 9, p. 093504, 2019.

[10] E. Hirvijoki *et al.*, "Ascot: Solving the kinetic equation of minority particle species in tokamak plasmas," *Computer Physics Communications*, vol. 185, no. 4, pp. 1310–1321, 2014.

[11] J. Varje *et al.*, "High-performance orbit-following code ascot5 for monte carlo simulations in fusion plasmas," *arXiv*, 2019.

[12] S. A. Lazerson *et al.*, "First neutral beam experiments on wendelstein 7-x," *Nuclear Fusion*, vol. 61, no. 9, p. 096008, jul 2021.

[13] S. P. Hirshman and J. C. Whitson, "Steepest-descent moment method for three-dimensional magnetohydrodynamic equilibria," *The Physics of Fluids*, vol. 26, no. 12, pp. 3553–3568, 1983.

[14] S. A. Lazerson, "The virtual-casing principle for 3d toroidal systems," *Plasma Physics and Controlled Fusion*, vol. 54, no. 12, p. 122002, nov 2012.

[15] N. Rust, B. Heinemann, B. Mendelevitch, A. Peacock, and M. Smirnow, "W7-x neutral-beam-injection: Selection of the nbi source positions for experiment start-up," *Fusion Engineering and Design*, vol. 86, no. 6, pp. 728–731, 2011, proceedings of the 26th Symposium of Fusion Technology (SOFT-26).

[16] M. McMillan and S. A. Lazerson, "BEAMS3d neutral beam injection model," *Plasma Physics and Controlled Fusion*, vol. 56, no. 9, p. 095019, jul 2014.

[17] S. A. Lazerson *et al.*, "Validation of the BEAMS3d neutral beam deposition model on wendelstein 7-x," *Nuclear Fusion*, vol. 60, no. 7, p. 076020, jun 2020.

[18] S. A. Lazerson, "Modeling and measurement of energetic particle slowing down in wendelstein 7-x," *Nuclear Fusion*, vol. 61, no. 9, p. 096005, jul 2021.

[19] D. Kulla *et al.*, "Placement of a fast ion loss detector array for neutral beam injected particles in wendelstein 7-x," *Plasma Physics and Controlled Fusion*, 2021.

[20] J. Galdon-Quiroga *et al.*, "Velocity-space sensitivity and tomography of scintillator-based fast-ion loss detectors," *Plasma Physics and Controlled Fusion*, vol. 60, no. 10, p. 105005, aug 2018.
[21] J. Ongena *et al.*, "The icrh system for the stellarator wendelstein 7-x," *AIP Conference Proceedings*, vol. 2254, no. 1, p. 070003, 2020.